CMS Physics Analysis Summary

Contact: cms-pag-conveners-exotica@cern.ch 2015/03/17

Search for a massive resonance decaying into a Higgs boson and a W or Z boson in hadronic final states in proton-proton collisions at $\sqrt{s} = 8$ TeV

The CMS Collaboration

Abstract

A search for a massive resonance decaying into a standard model Higgs boson (H) and a W or Z boson is reported. The analysis is performed on a data sample corresponding to an integrated luminosity of 19.7 fb^{-1}, collected in proton-proton collisions at a centre-of-mass energy of 8 TeV with the CMS detector at the LHC. Signal events in which the decay products of Higgs, W or Z bosons at high Lorentz boost are contained within a single reconstructed jet are identified using jet substructure techniques, including the tagging of b hadrons. This is the first search for heavy resonances decaying into HW or HZ resulting in an all-jets final state, as well as the first application of jet substructure techniques to identify $H \to WW^* \to 4q$ decays at high Lorentz boost. No significant signal is observed and limits are set at the 95% confidence level on the production cross section of W′ and Z′ in a model with mass-degenerate charged and neutral spin-1 resonances. Resonance masses are excluded for W′ in [1.0, 1.6] TeV, for Z′ in [1.0, 1.1], [1.3,1.5] TeV, and for mass-degenerate W′ and Z′ in [1.0, 1.7] TeV ranges.

1 Introduction

Several physics models beyond the standard model (SM) predict the existence of vector resonances with masses above 1 TeV that decay into a W or Z vector boson (V) and a SM Higgs boson (H) [1, 2]. Here we present a search for the production of such resonances in proton-proton (pp) collisions at a centre-of-mass energy of $\sqrt{s} = 8$ TeV. The data sample, corresponding to an integrated luminosity of 19.7 fb^{-1}, was collected with the CMS detector at the CERN LHC.

The composite Higgs [3–5] and little Higgs models [6–8] provide a direct solution to the hierarchy problem and predict many new particles, including additional gauge bosons, e.g. heavy spin-1 W′ or Z′ bosons (V′). These models can be generalized in the heavy vector triplet (HVT) framework [9]. Of particular interest for this search is the so called HVT scenario B model, where the branching fractions $\text{BR}(\text{W}' \to \text{WH})$ and $\text{BR}(\text{Z}' \to \text{ZH})$ dominate over the corresponding branching fractions to fermions, and are comparable to $\text{BR}(\text{W}' \to \text{WZ})$ and $\text{BR}(\text{Z}' \to \text{WW})$. In this scenario, experimental constraints from searches for the decay channels to bosons are more stringent than those sensitive to the decay channels to fermions. Specific searches for $\text{W}' \to \text{WZ}$ have been reported [10–14], excluding resonance masses below 1.7 TeV, quoted in terms of the Extended Gauge Boson reference model [15] with enhanced couplings to fermions as opposed to the HVT scenario B model. In addition, model independent limits from the $\ell\nu$+jets final state that can be used to set limits on $\text{W}' \to \text{WZ}$ and $\text{Z}' \to \text{WW}$ resonances have been reported in Ref. [16], corresponding to limits of approximately 1.7 TeV and 1.1 TeV on the W′ and Z′ masses respectively. A search for $\text{Z}' \to \text{ZH} \to \text{q}\bar{\text{q}}\tau\tau$ was reported in Ref. [17] and interpreted in the context of HVT scenario model B, however, no resonance mass limit could be set with the given sensitivity.

The signal of interest is a heavy vector resonance V′ decaying into HV, where the V decays to a pair of quarks and the H decays either to a b quark pair or to a pair of W bosons, which further decay into quarks. In pp collisions at the LHC, the momenta of the H and V emerging from the V′ boson decay are usually high enough that the hadronization products of H or V decay are reconstructed as a single jet [18]. For example, the final state hadrons from the $\text{V} \to \bar{\text{q}}\text{q}'$ decay merge into a single jet for V boson momenta above ~ 200 GeV; for this reason, for the V′ resonance masses of interest, the V′→HV decay results in a dijet event topology, and the traditional analysis techniques relying on resolved jets are no longer applicable. The signal is characterized by a peak in the dijet invariant mass distribution (m_{jj}) over a continuous background from mainly QCD multijet events. The sensitivity to jets from H decays to b quark pairs is enhanced through subjet or jet b tagging [19]. Jets from $\text{H} \to \text{WW}^* \to 4\text{q}$ decays, and also jets from W/Z bosons, are identified with jet substructure techniques [20, 21].

This is the first search for heavy resonances decaying into HV resulting in an all-jets final state, as well as the first application of jet substructure techniques to identify $\text{H} \to \text{WW}^* \to 4\text{q}$ decays of the H at a high Lorentz boost.

2 The CMS detector

The central feature of the CMS apparatus is a superconducting solenoid of 6 m internal diameter, providing a magnetic field of 3.8 T. Within the field volume are a silicon pixel and strip tracker, a lead tungstate crystal electromagnetic calorimeter, and a brass and scintillator hadron calorimeter, each composed of a barrel and two endcap sections. Muons are measured in gas-ionization detectors embedded in the steel flux-return yoke outside the solenoid. Extensive forward calorimetry complements the coverage provided by the barrel and endcap detectors. A more detailed description of the CMS detector, together with a definition of the coordinate

system used and the relevant kinematic variables, can be found in Ref. [22].

3 Signal model and simulation

In the HVT framework, the production cross sections of W′ and Z′ bosons and their decay branching fractions depend on three parameters in addition to the resonance masses: the strength of couplings to quarks (c_q), the H (c_H), and their self-coupling (g_V). In the HVT model B, where $g_V = 3$ and $c_q = -c_H = 1$, W′ and Z′ preferentially couple to bosons (W/Z/H), giving rise to di-boson final states. This feature reproduces the properties of the W′ and Z′ bosons predicted by composite Higgs model. In this case, the production cross sections for Z′, W'^-, and W'^+ are respectively 165, 87, and 248 fb for the signal of resonance mass $m_{V'} = 1$ TeV. Their branching fractions to VH and decay width are respectively 51.7%, 50.8%, 50.8% and 35.0, 34.9, 34.9 GeV. The natural width of the resonances is assumed to be smaller than the experimental resolution of m_{jj} for masses considered in this analysis.

We consider the W′ and Z′ resonances separately, and report individual limits for each candidate, allowing the reinterpretation of our results in different scenarios with a different number of spin-1 resonances.

The signals of interest are generated using the MADGRAPH 5.1.5.11 [23] Monte Carlo (MC) event generator with input parameters provided in Ref. [24], with an H mass of 125 GeV, processed through a simulation of the CMS detector, based on GEANT4 [25]. Simulated events showered with PYTHIA 6.426 [26] are used in the analysis. Samples from HERWIG++ 2.5.0 [27] are used to evaluate the systematic uncertainty by studying the difference of hadronization with the samples showered with PYTHIA. Tune Z2* [28] is used in PYTHIA, while the version 23 tune [27] is used in HERWIG++. The CTEQ6L1 [29] parton distribution functions (PDF) are used for PYTHIA and HERWIG++. Signal events are generated from resonance mass 1.0 TeV to 2.6 TeV in steps of 0.1 TeV, and the signals with intermediate resonance masses between the generated samples are interpolated.

4 Event reconstruction and selection

The event selection, in the online trigger as well as offline, utilizes a global event description by combining information from the individual subdetectors. Online, events are selected by at least one of two specific triggers, one based on the scalar sum of the transverse momenta p_T of the jets, and the other on the invariant mass of the two jets with highest p_T. The offline reconstruction is described below.

Events must have at least one primary vertex reconstructed with $|z| < 24$ cm. The primary vertex used in the event reconstruction is the one with the largest summed p_T^2 of associated tracks. Individual particle candidates are reconstructed and identified using the particle-flow (PF) algorithm [30, 31], and divided into five categories: muons, electrons, photons (including those that convert into e^+e^- pairs), charged hadrons, and neutral hadrons. Charged PF candidates associated with a different primary vertex are discarded, which reduces the contamination from additional pp interactions in the same bunch crossings (pileup). Jets are clustered from the remaining PF candidates, except those identified as isolated muons, using the Cambridge–Aachen (CA) [32, 33] jet clustering algorithm as implemented in FASTJET [34, 35]. A distance parameter of 0.8 is used for the CA algorithm (CA8 jets). An event-by-event correction based on the jet area method [36–38] is applied to remove the remaining energy deposited by neutral particles originating from pileup. The pileup-subtracted jet four-momenta are then corrected

to account for the difference between the measured and true energies of hadrons [38]. Jet identification criteria [39] are applied to the two highest p_T jets in order to remove spurious events associated with calorimeter noise. The jet reconstruction efficiencies (estimated from simulation) are larger than 99.9%, and contribute negligibly to the systematic uncertainties for signal events.

Events are selected by requiring at least two jets each with $p_T > 30\,\text{GeV}$ and $|\eta| < 2.5$. The two highest p_T jets are required to have a pseudorapidity separation $|\Delta\eta| < 1.3$ to reduce background from multijet events [40]. The invariant mass of these two jets is required to satisfy $m_{jj} > 890\,\text{GeV}$. The trigger efficiency for the events passing the preselection requirements exceeds 99%.

To enable reinterpretation of the results in models with different acceptances, in the following we provide the global efficiency approximated by the product of acceptances and the W/Z/H tagging efficiency, restricted to final states where the W, Z and H bosons decay hadronically. A matching of the generated W, Z and H bosons, and their reconstructed single jets is required within $\Delta R = \sqrt{(\Delta\eta)^2 + (\Delta\phi)^2} < 0.5$ as a part of the acceptances. The products of acceptances and the W/Z/H tagging efficiencies, ignoring leptonic decays and the correlations between detector acceptance and W/Z/H tagging, agree to better than 10% with the full event simulation. In the interpretations reported in this paper, the global efficiency is estimated from the full simulation of signal events, without applying the matching requirement. In this way, the correlations between the acceptance and W/Z/H tagging efficiency are properly taken into account. However, when interpreting this search in terms of W/Z/H tagging efficiency for an arbitrary model an additional uncertainty of 10% should be taken into account.

The acceptance, shown in Fig. 1 as a function of the dijet resonance mass for several signals, takes into account the angular acceptance ($|\eta| < 2.5$, $|\Delta\eta| < 1.3$) and the matching.

The two highest p_T jets are chosen as hadronically decaying W/Z/H boson candidates and a tagging algorithm based on jet substructure is applied. As the mass of the V or H boson is larger than the mass of a typical QCD jet, the jet mass is the primary observable that distinguishes such a jet from a QCD jet. The bulk of the V or H jet mass arises from the kinematics of the two or more jet cores that correspond to the decay quarks. In contrast, the QCD jet mass arises mostly from soft gluon radiation. For this reason, the use of jet pruning [41, 42] improves discrimination by removing the softer radiation, as this shifts the jet mass of QCD jets to smaller values, while maintaining the jet mass for V and H jets close to the masses of Z, W or H bosons. Jet pruning is implemented as additional cuts in the process of CA jet clustering. This algorithm starts from a set of "protojets" given by the PF particles that form the original CA jet within a cone of $R = 0.8$. These protojets are iteratively combined with each other until a set of jets is found, however the large angle and low p_T protojets are removed in the process. The details of this procedure are given in [21]. The distributions of the pruned jet mass (m_j) for simulated signal and background samples, are shown in Fig. 2. Jets from boosted W and Z decays are expected to generate peaks at $m_j \approx 80$ and $m_j \approx 90\,\text{GeV}$, respectively. Jets from boosted H decays are expected to peak at $m_j \approx 120$ GeV. Hadronic top-quark jets, where the b quark and the two different light quarks from the $t \to Wb \to q\bar{q}'b$ decay are required to be within a reconstructed jet of size R = 0.8, peak at $m_j \approx 175$ GeV. Jets from multijet events and not-fully-merged W, Z and H bosons give rise to a peak around 20 GeV, whose size depends particularly on the spin and polarization of the boson. All peaks are slightly shifted to lower masses, due to removal of soft radiation by jet pruning. If the pruned jet has a mass (m_j) within $70 < m_j < 100\,\text{GeV}$ ($110 < m_j < 135\,\text{GeV}$), it is tagged as a W/Z (H) candidate.

Jet pruning can also provide a good delineation of subjets within the CA8 jet. To tag jets from

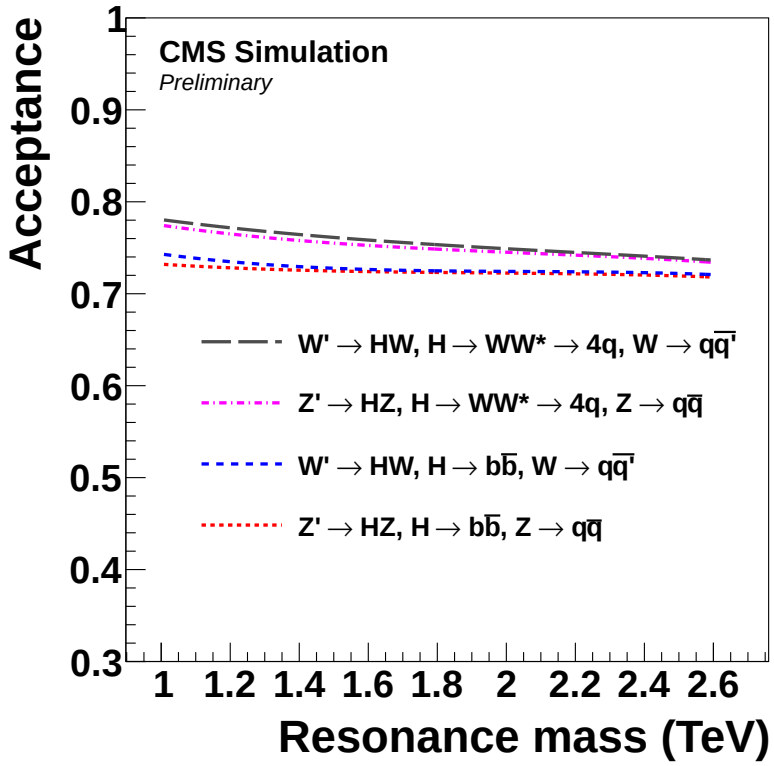

Figure 1: The fraction of simulated signal events for hadronically decaying W/Z/H bosons, reconstructed as two jets, that pass the geometrical acceptance criteria ($|\eta| < 2.5$, $|\Delta\eta| < 1.3$), shown as a function of the dijet invariant mass.

$H \to b\bar{b}$ decays, denoted as H_{bb} jets, the pruned subjets, given by reversing the last step of the CA8 pruning recombination algorithm, are used as the basis for b tagging. Jets arising from the hadronization of b quarks (b jets) are identified using the combined secondary vertex (CSV) b tagging algorithm [43], which uses information from tracks and secondary vertices associated with jets to build a likelihood-based discriminator to distinguish between jets from b quarks and those from charm or light quarks and gluons. The b tagging discriminator can take values between 0 and 1 with higher values indicating higher probability of the jet to originate from a b quark. The loose working point of the CSV algorithm [43] is chosen, which is found to be optimal for both subjets and jets b tagging. It gives a b-tagging efficiency of $\approx 85\%$, with mistagging probabilities of $\approx 40\%$ for c-quark jets and $\approx 10\%$ for light-quark and gluon jets with $p_T \approx 80$ GeV. The b-tagging efficiency ratio between data and simulation is applied as a scale factor [19] to the simulated signal events. To identify CA8 jets originating from H decays resulting in two collimated b jets, we apply b tagging either on the two subjets or the CA8 jet, based on the angular separation of the two subjets (ΔR) [19]. If ΔR between the CA8 subjets is bigger (smaller) than 0.3, b tagging is applied on both of the two subjets (on the CA8 jet).

In $H \to WW^* \to 4q$ decays, the boosted H will decay into one real W boson and one virtual W boson, resulting in a final state of four quarks merged together, denoted as an H_{WW} jet. In addition to the pruned jet mass selection, in tagging jets arising from $H \to WW^* \to 4q$ and $W/Z \to \bar{q}q'$ decays we achieve additional discrimination against multijet events by considering the distribution of jet constituents relative to the jet axis. In particular, we quantify how well the constituents of a given jet can be arranged into N subjets. This is done by reconstruct-

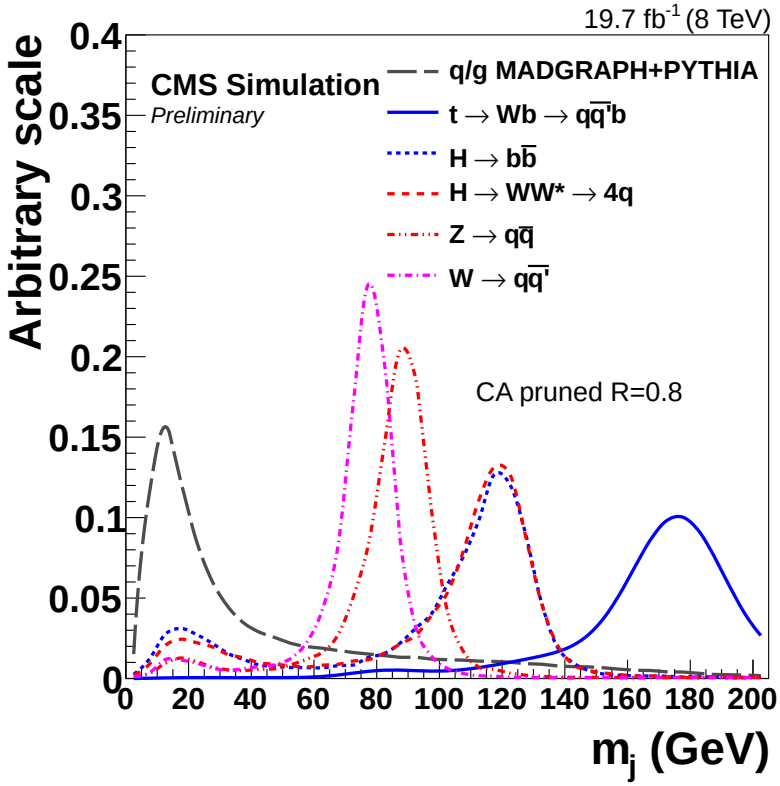

Figure 2: Distribution of pruned jet mass in simulation of signal and background processes. All simulated distributions are normalized to 1. The W/Z/H and top-quark jets are required to match respective generator level particles in the event. The W/Z/H jets are from 1.5 TeV $W' \to WH$ and $Z' \to ZH$ signal samples.

ing the full set of jet constituents (before pruning) with the k_T algorithm [44] and halting the reclustering when N distinguishable protojets are formed. The directions of the N jets are used as the reference axes to compute the N-subjettiness [45–47] τ_N of the original jet, defined as

$$\tau_N = \frac{1}{d_0} \sum_k p_{T,k} \min(\Delta R_{1,k}, \Delta R_{2,k}, \ldots, \Delta R_{N,k}), \quad (1)$$

where $p_{T,k}$ is the p_T of the k^{th} constituent of the original jet and $\Delta R_{n,k}$ is its angular distance from the axis of the n^{th} subjet (with $n = 1, 2, \ldots, N$). The normalization factor d_0 for τ_N is $d_0 = \sum_k p_{T,k} R_0$, with R_0 set to the distance parameter $R = 0.8$ of the original CA8 jet. To improve the discriminating power, we perform a one-pass optimization of the directions of the subjets' axes by minimizing τ_N [21, 46]. By using the smallest $\Delta R_{n,k}$ to weight the value of $p_{T,k}$ in Eq. (1), τ_N yields small values when the jet originates from the hadronization of N or fewer quarks. The $\tau_{ij} = \tau_i / \tau_j$ ratios τ_{21}, τ_{31}, τ_{32}, τ_{41}, τ_{42}, and τ_{43} have been studied to identify the best discriminators for jets from $H \to WW^* \to 4q$ and $W/Z \to \bar{q}q'$ decays. We find that the ratio τ_{42} works best to discriminate the four-pronged $H \to WW^* \to 4q$ events against QCD jets, and τ_{21} to identify $W/Z \to \bar{q}q'$ [48].

The discriminating power of τ_{42} can be seen in Fig. 3. The τ_{42} distribution of H_{WW} jets tends to peak around 0.55. By contrast, τ_{42} distributions of multijet background and W/Z jets have a larger fraction of events at large values of τ_{42}, especially after requiring a pruned jet mass in the range [110, 135] GeV. Jets from unmatched $t\bar{t}$ events peak together with QCD jets. However, the

τ_{42} distribution for matched top-quark jets tends to peak at smaller values, since for the same jet τ_{42} is nearly always less than τ_{32}, which is small for hadronic top-quark jets.

In Fig. 3, the comparison between dijet data and the QCD multijet simulation shows that the simulated distribution is well reproduced, though shifted towards higher values of τ_{42} compared to the data. A similar level of disagreement is known for the modeling of τ_{21} in QCD simulation in Ref. [14]. The disagreement does not affect this analysis since the background is estimated from data. For the signal scale factor, the uncertainties from the modelling of τ_{42} are taken into account.

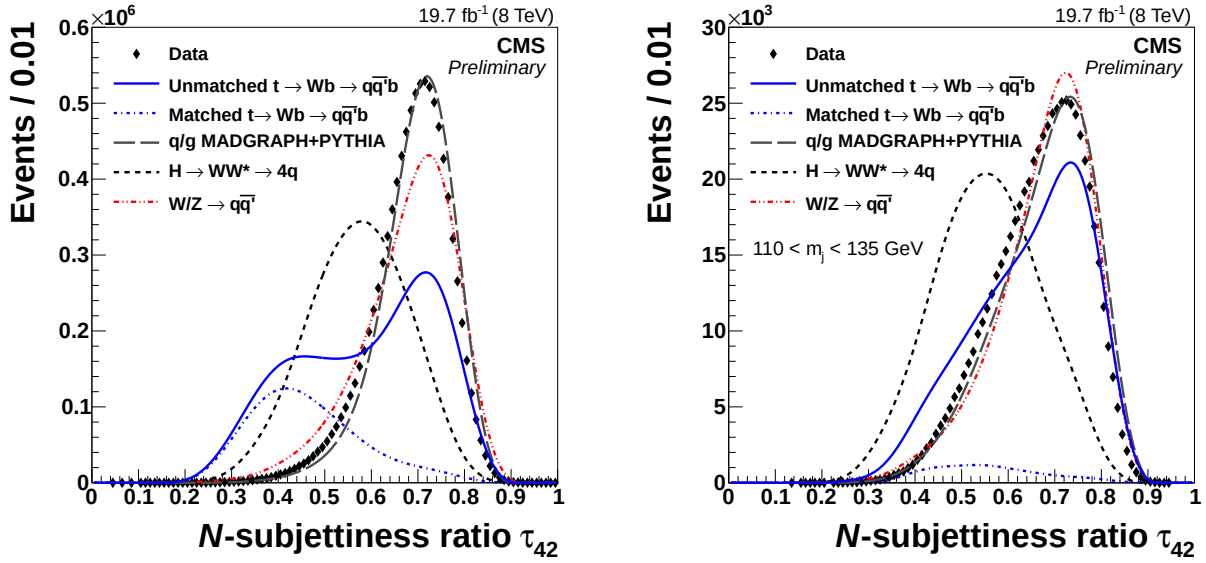

Figure 3: Distributions of τ_{42} in data and in simulations of signal (2 TeV) and background events, without applying the pruned jet mass requirement (left) and with the pruned jet mass requirement applied (right). W/Z, matched top-quark, and H_{WW} jets are required to match their generator level particles, respectively. All simulated distributions are scaled to match the number of events in data, except that matched top-quark background is scaled to the fraction of unmatched $t\bar{t}$ events times the number of data events.

We select "high (low)-purity" W/Z jets by requiring $\tau_{21} \leq 0.5$ ($0.5 < \tau_{21} < 0.75$), denoted as HP (LP) V tag. We select HP (LP) H_{WW} jets by requiring $\tau_{42} \leq 0.55$ ($0.55 < \tau_{42} < 0.65$), denoted as HP (LP) H tag.

Cross-talk between the H decay channels is possible; for example, two-pronged H decays (e.g. $H \to b\bar{b}$, $H \to c\bar{c}$) can be reconstructed as four-pronged $H \to WW^* \to 4q$, as shown in Fig. 4. Because of its large branching fraction, $H \to b\bar{b}$ contributes a non-negligible number of events to the $H \to WW^* \to 4q$ tagged sample. In order to combine events from $H \to b\bar{b}$ and $H \to WW^* \to 4q$ channels into a single joint likelihood, these categories must be mutually exclusive. Since the $H \to b\bar{b}$ tagger has significantly lower background than $H \to WW^* \to 4q$, it takes precedence in selecting events. We first identify the events that pass the $H \to b\bar{b}$ tagger, and only if they fail, we test them for the presence of the $H \to WW^* \to 4q$ tag. Thus we arrive at the final division of events into mutually exclusive categories. This is summarized in Table 1.

The LP V tag and LP H tag category is not included in this analysis, since it is dominated by background and therefore its contribution to the expected significance of the signal is negligible. Other H decay modes like $H \to gg$, $H \to \tau\tau$, $H \to ZZ^*$, and $H \to c\bar{c}$ all together contribute $2\% - 7\%$ of the total $H \to b\bar{b}$ tagged events, and $18\% - 24\%$ of the total $H \to WW^* \to 4q$ tagged

Table 1: Summary of event categories and their nomenclature used in the paper.

VH_{bb}	VH_{WW}
HP V tag ($V^{HP}H_{bb}$)	HP H and V tag ($V^{HP}H^{HP}_{WW}$)
LP V tag ($V^{LP}H_{bb}$)	HP H tag and LP V tag ($V^{LP}H^{HP}_{WW}$)
	HP V tag and LP H tag ($V^{HP}H^{LP}_{WW}$)

events, as shown in Fig. 4. In this analysis, we only consider the $H \to b\bar{b}$ and $H \to WW^* \to 4q$ channels. Other H channels passing the taggers are conservatively viewed as background and included as systematic uncertainties, discussed in Section 6.

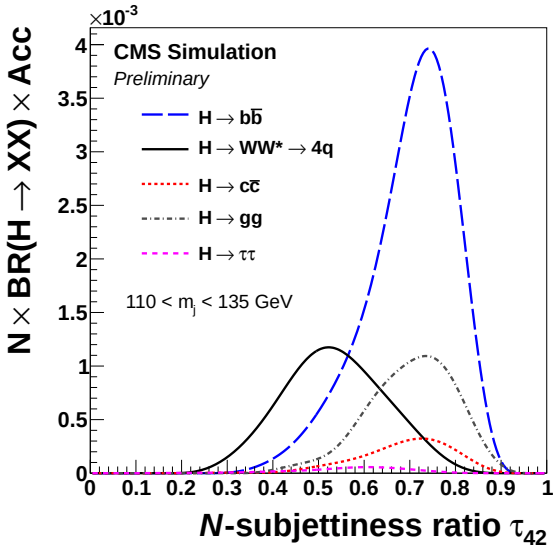

Figure 4: Comparison of τ_{42} distributions for $H \to WW^* \to 4q$, $H \to b\bar{b}$, $H \to gg$, $H \to c\bar{c}$, and $H \to \tau\tau$ channels failing the $H \to b\bar{b}$ requirement. The H jets are from HV signals with a 1.5 TeV resonance. All curves are normalized to the product of the corresponding branching fraction and acceptance.

The expected tag probabilities of the W, Z, and H selection criteria for signal and data events in different event categories are shown in Figs. 5 and 6, as a function of m_{jj}. The W/Z and $H \to WW^* \to 4q$ tagging efficiencies for signal events in the HP categories drop at high p_T, primarily because the τ_{21} and τ_{42} distributions are p_T-dependent.

The MC modelling of V-tag efficiency is validated using high-p_T $W \to \bar{q}q'$ decays selected from a data sample enriched in semileptonic $t\bar{t}$ events [21]. Scale factors of 0.86 ± 0.07 and 1.39 ± 0.75 are applied to the MC events in the HP and LP V tag categories, respectively, to match the tagging efficiencies in top pair production data. The decay of $H \to WW^* \to 4q$ produces a hard W jet accompanied by two soft jets from the off-shell W boson. As the $H \to WW^* \to 4q$ tagger is also based on the N-subjettiness variables, and the ratio τ_{42}/τ_{21} in data peaks at ≈ 1 which is well modeled by QCD simulation, it is reasonable to assume that the mismodeling of the shower by PYTHIA is similar to that in the case of V tagging. The $H \to WW^* \to 4q$ tagging efficiency scale factors are extrapolated using the same technique as for V tagging for both the HP and LP categories, respectively, with additional systematic uncertainties, which are discussed in Section 6.

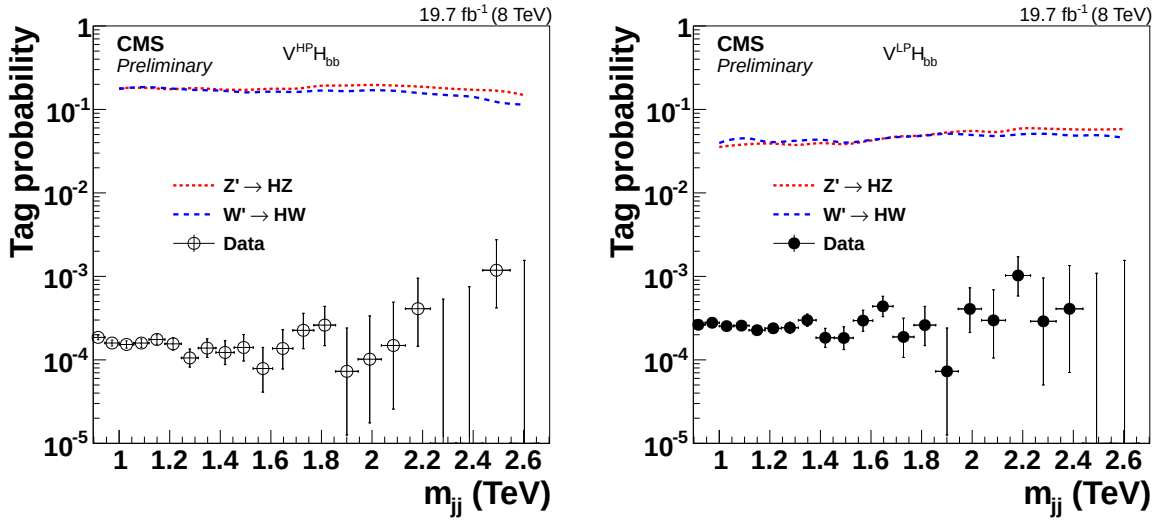

Figure 5: Tag probabilities in $H \to b\bar{b}, W/Z \to \bar{q}q'$ signal channels and data, for categories of $V^{HP}H_{bb}$ (left), and $V^{LP}H_{bb}$ (right). Horizontal bars in data indicates the bin width.

5 Resonance search in the dijet mass spectrum

The resolution for the m_{jj} reconstruction is around 5% − 10% for all the five categories. The background from multijet events is modelled by a smoothly falling distribution for each event category, given by the empirical probability density function

$$P_D(m_{jj}) = \frac{P_0(1 - m_{jj}/\sqrt{s})^{P_1}}{(m_{jj}/\sqrt{s})^{P_2}} . \tag{2}$$

For each category, the normalization factor P_0 and the two shape parameters P_1 and P_2 are treated as uncorrelated. This parameterization was deployed successfully in a number of searches based on dijet mass spectra [40]. A Fisher F-test [49] is used to check that no additional parameters are needed to model the individual background distributions, compared with the four-parameter function used in [40]. We have also tested an alternative function $P_E(m_{jj}) = \frac{P_0}{(m_{jj}/\sqrt{s}+P_1)^{P_2}}$, and found it less favored by the F-test. The changes in the result are negligible so no additional systematic uncertainty is assigned for this.

We search for a peak on top of the falling background spectrum by means of a binned maximum likelihood fit to the data. The binned likelihood is given by

$$\mathcal{L} = \prod_i \frac{\lambda_i^{n_i} e^{-\lambda_i}}{n_i!}, \tag{3}$$

where $\lambda_i = \mu N_i(S) + N_i(B)$, μ is a scale factor for the signal, $N_i(S)$ is the number of events expected from the signal, and $N_i(B)$ is the number expected from multijet background. The variable n_i quantifies the number of observed events in the i^{th} m_{jj} bin. The number of background events $N_i(B)$ is described by the functional form of Eq. (2). While maximizing the likelihood, μ as well as the parameters of the background function are unconstrained and left floating. For presentational purposes a binning according to m_{jj} resolution is used in this paper. However, the likelihood is calculated in bins of 1 GeV in m_{jj}, approximating an unbinned analysis, while keeping it computationally manageable.

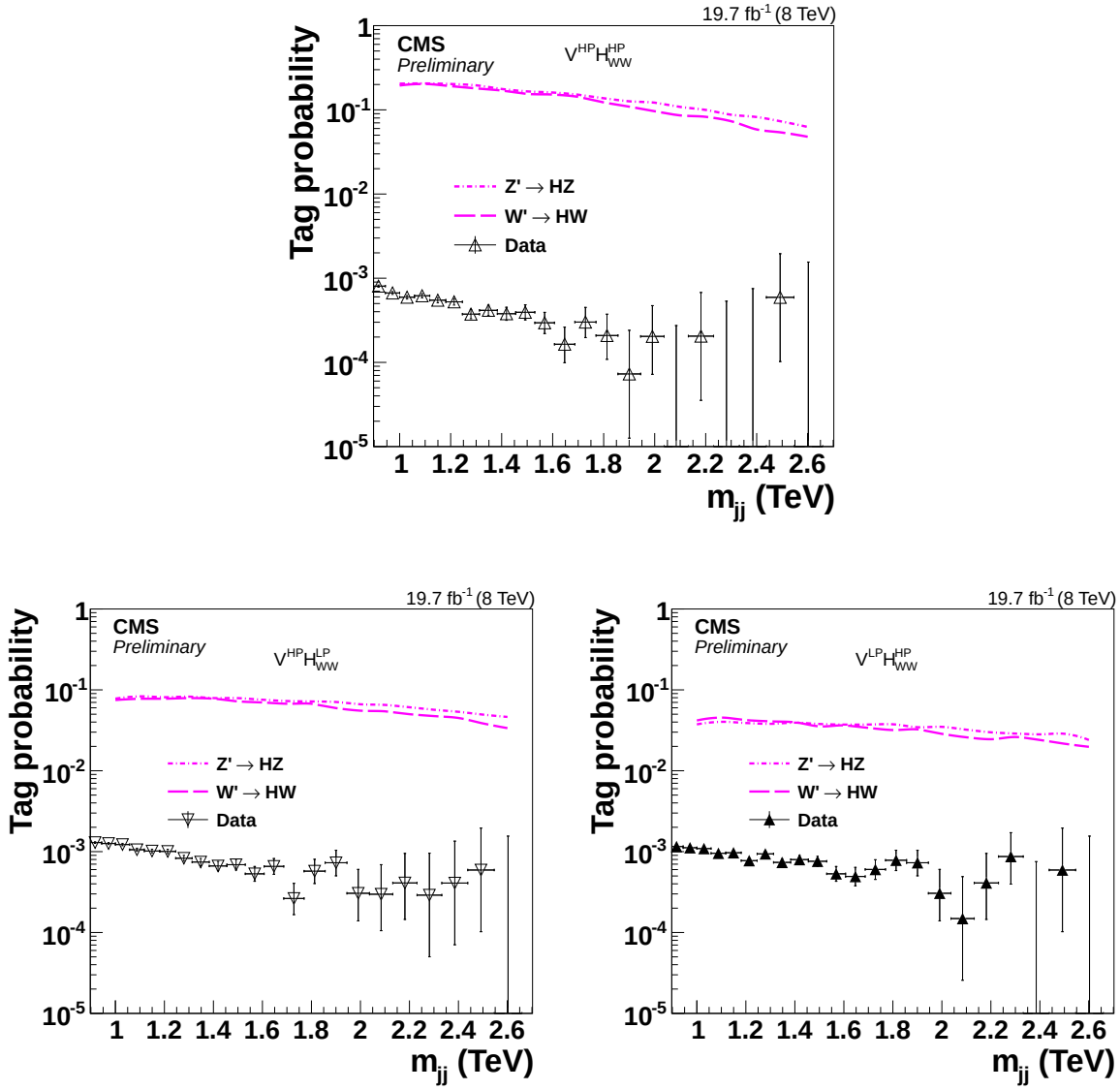

Figure 6: Tag probabilities in $H \to WW^* \to 4q, W/Z \to \bar{q}q'$ signal channels and data, for categories of $V^{HP}H^{HP}_{WW}$ (top), $V^{HP}H^{LP}_{WW}$ (bottom left) and $V^{LP}H^{HP}_{WW}$ (bottom right). Horizontal bars in data indicates the bin width.

Figures 7 and 8 show the m_{jj} distributions in data, binned according to m_{jj} resolution. The solid curves represent the results of the maximum likelihood fit to the data, fixing the number of expected signal events to zero, while the bottom panels show the corresponding pull distributions, quantifying the agreement between the background-only hypothesis and the data. The expected distributions of $H \to b\bar{b}, W/Z \to \bar{q}q'$ and $H \to WW^* \to 4q, W/Z \to \bar{q}q'$ signals at 1.0, 1.5 and 2.0 TeV in each category, scaled to their corresponding cross sections are given by the dashed and dash-dotted curves. The resonance masses in VH_{bb} channels are slightly lower than that of the VH_{WW} channels because of missing neutrinos in b-hadron decays and partial misreconstruction of two-pronged $H \to b\bar{b}$ decay.

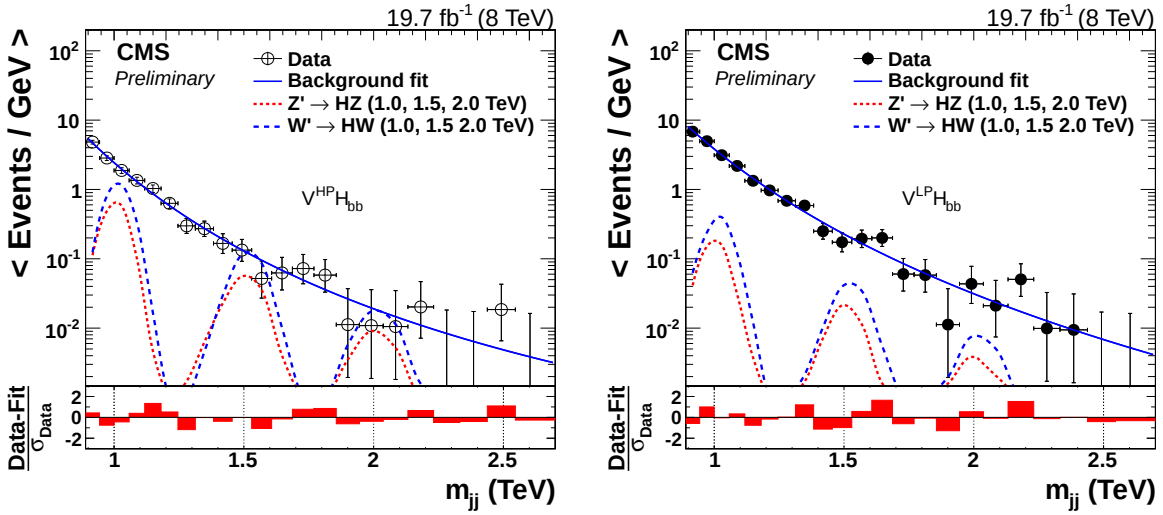

Figure 7: Distributions in m_{jj} are shown for $V^{HP}H_{bb}$ category (left), $V^{LP}H_{bb}$ category (right). The solid curves represent the results of fitting Eq. (2) to the data. The distributions for $H \to b\bar{b}, W/Z \to \bar{q}q'$contributions, scaled to their corresponding cross sections, are given by the dashed curves. Y axis displays the number of events per bin, divided by bin width. Horizontal bars in data indicates the bin width. The corresponding pull distributions ($\frac{\text{Data}-\text{Fit}}{\sigma_{\text{Data}}}$, where σ_{Data} represents the statistical uncertainty in the data in a bin in m_{jj}) are shown below each m_{jj} plot.

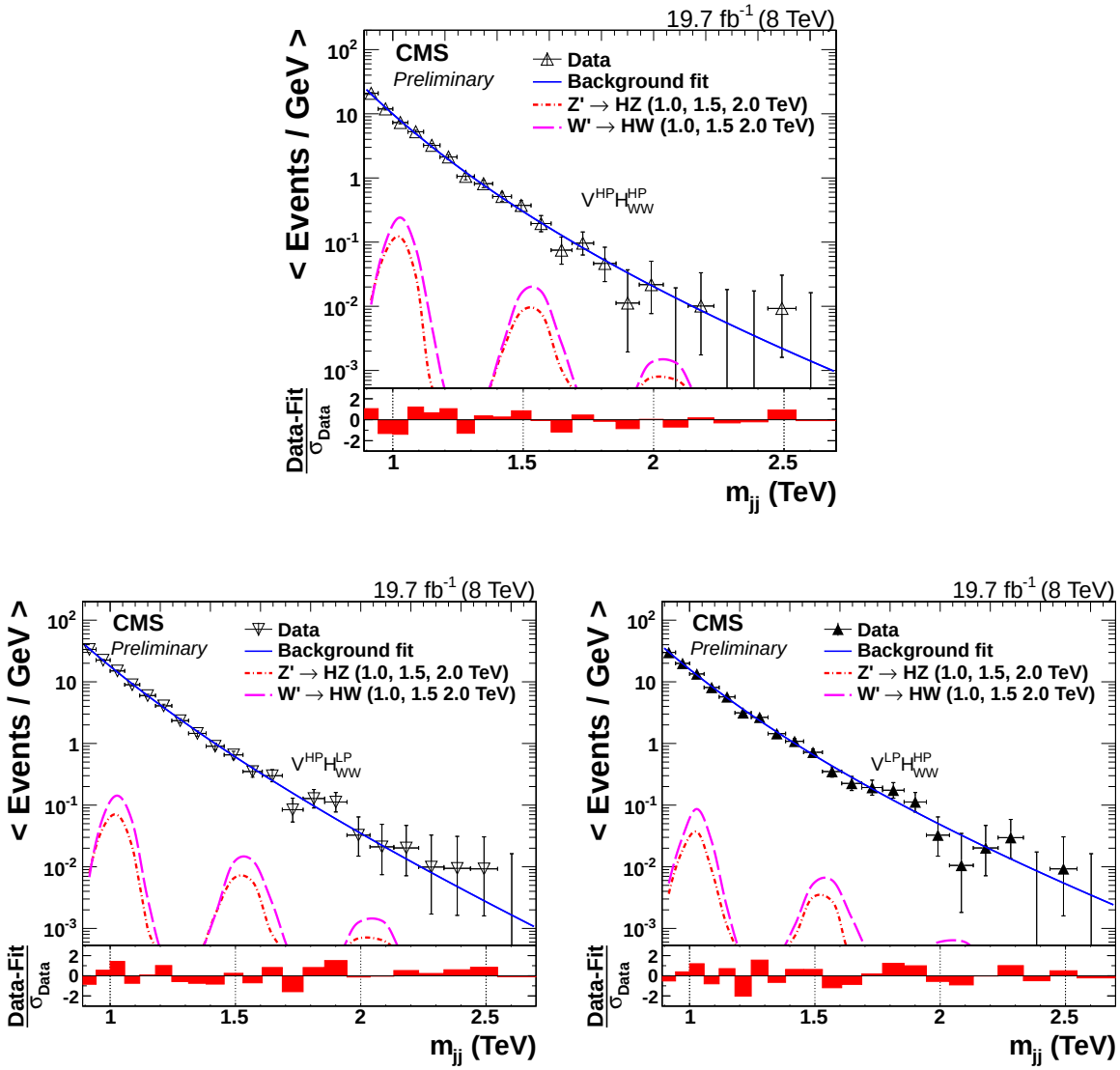

Figure 8: Distributions in m_{jj} are shown for $V^{HP}H^{HP}_{WW}$ (top), $V^{LP}H^{HP}_{WW}$ (bottom left), and $V^{HP}H^{LP}_{WW}$ (bottom right). The solid curves represent the results of fitting Eq. (2) to the data. The distributions for $H \to WW^* \to 4q, W/Z \to \bar{q}q'$ contributions, scaled to their corresponding cross sections, are given by the dashed and dash-dotted curves. Y axis displays the number of events per bin, divided by bin width. Horizontal bars in data indicates the bin width. The corresponding pull distributions ($\frac{\text{Data}-\text{Fit}}{\sigma_{\text{Data}}}$, where σ_{Data} represents the statistical uncertainty in the data in a bin in m_{jj}) are shown below each m_{jj} plot.

6 Systematic uncertainties

The largest contributions to the systematic uncertainty are associated with the modelling of the signal, namely the determination of the efficiencies of W/Z tagging, H tagging, and b tagging, choice of PDF, jet energy scale (JES), jet energy resolution (JER), pileup, cross-talk between different signal contributions, and integrated luminosity.

The uncertainty in the efficiency for W/Z-tagging is estimated using a control sample enriched with $t\bar{t}$ events described in Ref. [21]. Uncertainties of 7.5% and 54% in the respective scale factors for HP and LP V tag include contributions from control-sample statistical uncertainties, and the uncertainties in the JES and JER for pruned jets [48]. To extrapolate to higher jet p_T, an estimation of V tagging efficiency varying as a function of p_T for two different showering and hadronization models using PYTHIA 6 and HERWIG++, shows that the differences are within 4% (12%) for the HP (LP) V-tagging [21]. We extrapolate the $H \to WW^* \to 4q$ tagging efficiency scale factor in the same way as the W/Z-tagger, with an additional systematic uncertainty based on the difference between PYTHIA 6 and HERWIG++ in modelling $H \to WW^* \to 4q$ decay. This is evaluated to be ≈ 7 % for the HP and LP H tag. The uncertainty from the pruned jet mass requirement in the $H \to WW^* \to 4q$ search is already included in the extrapolated scale factor uncertainty of the V-tag.

The uncertainty in the efficiency of $H \to b\bar{b}$ tagging can be separated into two categories: the efficiency related to the b tagging and the efficiency related to the pruned H mass tag. The first is obtained by varying the b tagging scale factors within the associated uncertainties [19] and amounts to 15%. The second is assumed to be similar to the mass selection efficiency of W jets estimated in Ref. [21], additionally accounting for the difference in fragmentation of light quarks and b quarks, which amounts to 2.6% per jet.

Because of the rejection of charged particles not originating from the primary vertex, and the application of pruning, the dependence of the W/Z/H tagging efficiency on pileup is weak and the uncertainty in the modelling of the pileup distribution is $\leq 1.5\%$ per jet.

In this analysis, we only consider $H \to b\bar{b}$ and $H \to WW^* \to 4q$ decays. Other H decay channels that pass H taggers are viewed as nuisance signals, and a corresponding cross-talk systematic uncertainty is assigned. We evaluate this uncertainty as a ratio of expected nuisance signal events with respect to the total expected signal events, taking into account the branching fractions, acceptances and tagging efficiencies. The contamination from cross-talk is estimated to be $2\% - 7\%$ in the VH_{bb} categories, and $18\% - 24\%$ in the VH_{WW} categories, and we take the maximum as the uncertainty. The analysis is potentially 7% (24%) more sensitive than quoted, but since it is not clear how well the efficiency for the nuisance signals is understood, they are neglected, yielding a conservative limit on new physics. When the VH_{bb} and VH_{WW} categories are combined together, the 24% uncertainty becomes a small effect, based on a quantity as a measure of sensitivity suggested in Ref. [50] :

$$P = \frac{\mathrm{BR}(H \to XX) \times \epsilon_S}{1 + \sqrt{B}} \tag{4}$$

where $\mathrm{BR}(H \to XX)$ is the branching fraction for the H decay channel, ϵ_S is the signal tagging efficiency and B is the corresponding background yield. The values of P for each channel are shown in Table 2.

The JES has an uncertainty of 1–2% [38, 51], and its p_T and η dependence is propagated to the reconstructed value of m_{jj}, yielding an uncertainty of 1%, regardless of the resonance mass. The impact of this uncertainty on the calculated limits is estimated by changing the dijet mass

Table 2: Summary of the values P for a Z′ signal at 1.5 TeV resonance mass and the corresponding background yield in all five categories.

Signal/Categories	$V^{HP}H_{bb}$	$V^{LP}H_{bb}$	$V^{HP}H^{HP}_{WW}$	$V^{HP}H^{LP}_{WW}$	$V^{LP}H^{HP}_{WW}$
$H \to b\bar{b}, Z \to q\bar{q}$	2.3×10^{-2}	4.8×10^{-3}	1.0×10^{-3}	1.6×10^{-3}	3.9×10^{-4}
$H \to WW^* \to 4q, Z \to q\bar{q}$	5.6×10^{-4}	≈ 0	2.6×10^{-3}	9.8×10^{-4}	4.5×10^{-4}

in the analysis within its uncertainty. The JER is known to a precision of 10%, and its non-Gaussian features observed in data are well described by the CMS simulation [38]. The effect of the JER uncertainty on the limits is also estimated by changing the reconstructed resonance width within its uncertainty. The integrated luminosity has an uncertainty of 2.6% [52], which is also taken into account in the analysis. The uncertainty related to the PDF used to model the signal acceptance is estimated from the CT10 [53], MSTW08 [54], and NNPDF21 [55] PDF sets. The envelope of the upward and downward variations of the estimated acceptance for the three sets is assigned as uncertainty [56] and found to be 5 – 15% in the resonance mass range of interest. A summary of all systematic uncertainties is given in Table 3 and 4. Among these uncertainties, the JES and JER are applied as shape uncertainties, while others are applied as uncertainty in the event yield.

Table 3: Systematic uncertainties common to all categories.

Source	HP uncertainties (%)	LP uncertainties (%)
JES	1	1
JER	10	10
Pileup	≤ 3.0	≤ 3.0
PDF	5–15	5–15
Integrated luminosity	2.6	2.6
W-tagging	7.5	54
W tag p_T dependence	4	12

Table 4: Systematic uncertainties specific to each channel. Numbers in parentheses represent the uncertainty for the corresponding LP category. If LP has the same uncertainty as HP, only the HP uncertainty is presented here.

	Uncertainty (%) for $X \to HV$ signals, in which H decays to		
	$H \to b\bar{b}$		$H \to WW^* \to 4q$
Source/categories	VH_{bb}	VH_{WW}	VH_{WW}
$H \to b\bar{b}$ mass scale	2.6		-
H(4q)-tagging	-		7.5 (54)
H(4q)-tag τ_{42} extrapolation	-		7
Cross-talk	7		24
b-tagging	≤ 15		-

7 Results

The asymptotic approximation [57] of the LHC CL_s criterion [58, 59] is used to set upper limits on the cross section for resonance production. The dominant sources of systematic uncertain-

ties are treated as nuisance parameters associated with log-normal priors in those variables. For a given value of the signal cross section, the nuisance parameters are fixed to the values that maximize the likelihood, a method referred to as profiling. The dependence of the likelihood on parameters used to describe the background in Eq. (2) is treated in the same manner, and no additional systematic uncertainty is assigned to the parameterization of the background.

The HP and LP event categories of H tag (V tag) are combined into a common likelihood, with the two uncertainties in the H tag (V tag) efficiency considered to be anticorrelated between HP and LP tagging because events failing the HP τ_{42} (τ_{21}) selection migrate to the LP category and the fraction of events failing both HP and LP requirements is small compared to the HP and LP events. The branching fractions of $H \to WW^* \to 4q$ and $H \to b\bar{b}$ decays are taken as fixed values in joint likelihood. The remaining systematic uncertainties in the signal are fully correlated across all channels. The variables describing the background uncertainties are treated as uncorrelated. Figure 9 shows the observed and background-only expected upper limits on the production cross sections for Z′ and W′, including both $H \to b\bar{b}$ and $H \to WW^* \to 4q$ decays, computed at 95% confidence level (CL), with the predicted cross sections for the benchmark models overlaid for comparison. In the HVT model scenario B, W′ and Z′ are degenerate in resonance mass, thus we compute the limit on their combined cross section under this hypothesis, shown in Fig. 10. Table 5 shows the exclusion ranges on resonance masses.

Table 5: Summary of observed lower limits on resonance masses at 95% CL and their expected values, assuming a null hypothesis. The analysis is sensitive to resonances heavier than 1 TeV.

Process	Observed lower mass limit (TeV)	Expected lower mass limit (TeV)
$Z' \to HZ$	[1.0, 1.1], [1.3, 1.5]	1.3
$W' \to HW$	[1.0, 1.6]	1.7
$V' \to VH$	[1.0, 1.7]	1.9

8 Summary

A data sample corresponding to an integrated luminosity of 19.7 fb^{-1}collected in pp collisions at $\sqrt{s} = 8$ TeV with the CMS detector has been used to measure the W/Z- and H-tagged dijet mass spectra using the two leading jets within the pseudorapidity range $|\eta| < 2.5$ and with pseudorapidity separation $|\Delta\eta| < 1.3$. The QCD background is suppressed using jet substructure tagging techniques and/or b tagging, which identify boosted bosons decaying into hadrons. In particular, we use the invariant mass of pruned jets and the N-subjettiness ratios τ_{21} and τ_{42}, as well as b tagging applied to the subjets of the H jet, to discriminate against the initially overwhelming QCD background. The remaining QCD background is estimated from a fit to the dijet mass distributions using a smooth function. We have searched for the signal as a peak on top of the smoothly falling QCD background. No significant signal is observed. In HVT model B, a Z′ is excluded in resonance mass regions, [1.0, 1.1] and [1.3, 1.5] TeV, while a W′ is excluded in [1.0, 1.6] TeV. Mass degenerate W′ plus Z′ particle is excluded in [1.0, 1.7] TeV.

This is the first search for heavy resonances decaying into HV resulting in a hadronic final state, as well as the first application of jet substructure techniques to identify $H \to WW^* \to 4q$ decays of the H at high Lorentz boost.

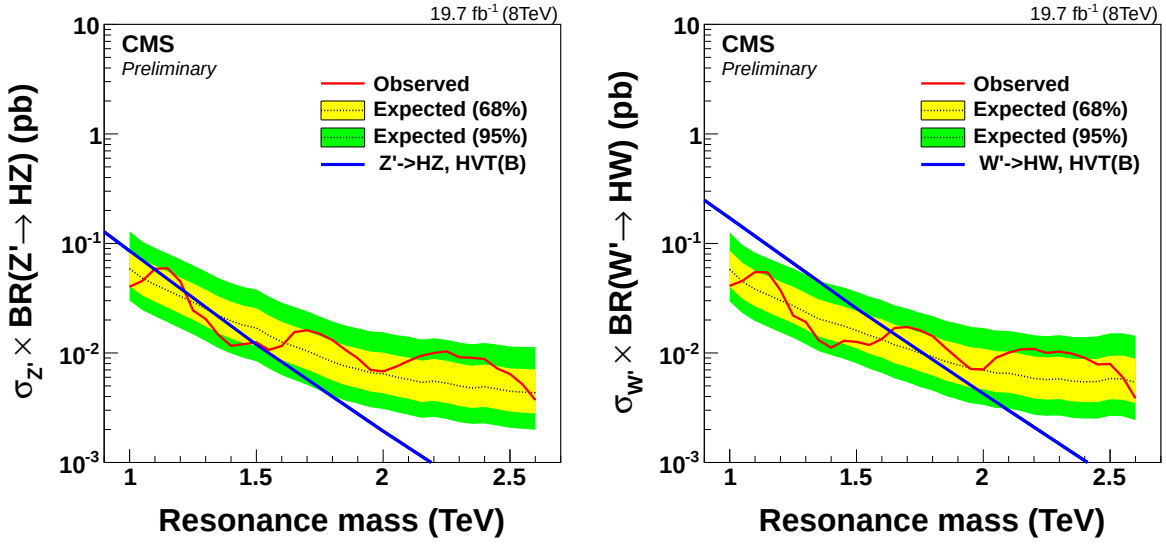

Figure 9: Expected and observed limits for $Z' \rightarrow HZ$ (left) and $W' \rightarrow HW$ (right),including all five categories. Branching fractions of H and V decays are already taken into account.

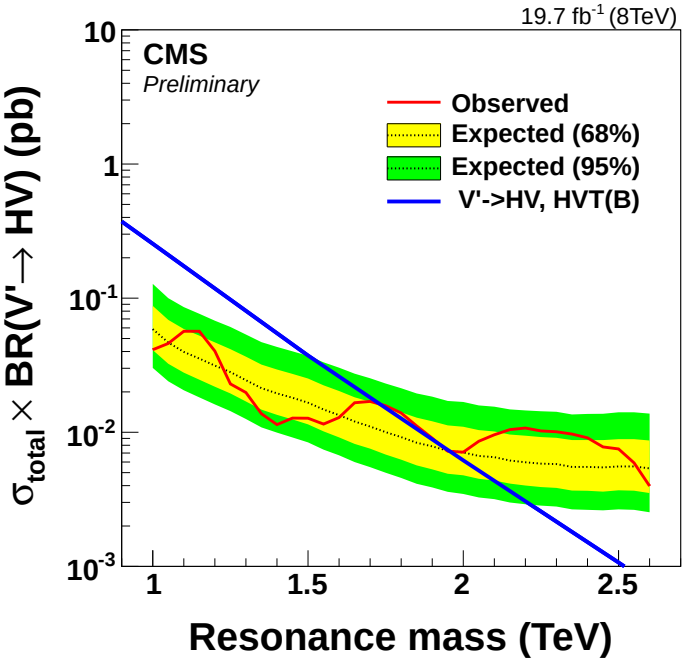

Figure 10: Expected and observed limits for $V' \rightarrow HV$ by combining W' and Z' together. Branching fractions of H and V decays are already taken into account.

Acknowledgements

We congratulate our colleagues in the CERN accelerator departments for the excellent performance of the LHC and thank the technical and administrative staffs at CERN and at other CMS institutes for their contributions to the success of the CMS effort. In addition, we gratefully acknowledge the computing centres and personnel of the Worldwide LHC Computing Grid for delivering so effectively the computing infrastructure essential to our analyses. Finally, we acknowledge the enduring support for the construction and operation of the LHC and the CMS detector provided by the following funding agencies: BMWFW and FWF (Austria); FNRS and FWO (Belgium); CNPq, CAPES, FAPERJ, and FAPESP (Brazil); MES (Bulgaria); CERN; CAS, MoST, and NSFC (China); COLCIENCIAS (Colombia); MSES and CSF (Croatia); RPF (Cyprus); MoER, ERC IUT and ERDF (Estonia); Academy of Finland, MEC, and HIP (Finland); CEA and CNRS/IN2P3 (France); BMBF, DFG, and HGF (Germany); GSRT (Greece); OTKA and NIH (Hungary); DAE and DST (India); IPM (Iran); SFI (Ireland); INFN (Italy); NRF and WCU (Republic of Korea); LAS (Lithuania); MOE and UM (Malaysia); CINVESTAV, CONACYT, SEP, and UASLP-FAI (Mexico); MBIE (New Zealand); PAEC (Pakistan); MSHE and NSC (Poland); FCT (Portugal); JINR (Dubna); MON, RosAtom, RAS and RFBR (Russia); MESTD (Serbia); SEIDI and CPAN (Spain); Swiss Funding Agencies (Switzerland); MST (Taipei); ThEPCenter, IPST, STAR and NSTDA (Thailand); TUBITAK and TAEK (Turkey); NASU and SFFR (Ukraine); STFC (United Kingdom); DOE and NSF (USA).

Individuals have received support from the Marie-Curie programme and the European Research Council and EPLANET (European Union); the Leventis Foundation; the A. P. Sloan Foundation; the Alexander von Humboldt Foundation; the Belgian Federal Science Policy Office; the Fonds pour la Formation à la Recherche dans l'Industrie et dans l'Agriculture (FRIA-Belgium); the Agentschap voor Innovatie door Wetenschap en Technologie (IWT-Belgium); the Ministry of Education, Youth and Sports (MEYS) of the Czech Republic; the Council of Science and Industrial Research, India; the HOMING PLUS programme of Foundation for Polish Science, cofinanced from European Union, Regional Development Fund; the Compagnia di San Paolo (Torino); the Consorzio per la Fisica (Trieste); MIUR project 20108T4XTM (Italy); the Thalis and Aristeia programmes cofinanced by EU-ESF and the Greek NSRF; and the National Priorities Research Program by Qatar National Research Fund.

References

[1] CMS Collaboration, "Observation of a new boson at a mass of 125 GeV with the CMS experiment at the LHC", *Phys. Lett. B* **716** (2012) 30, doi:10.1016/j.physletb.2012.08.021, arXiv:1207.7235.

[2] ATLAS Collaboration, "Observation of a new particle in the search for the Standard Model Higgs boson with the ATLAS detector at the LHC", *Phys. Lett. B* **716** (2012) 1, doi:10.1016/j.physletb.2012.08.020, arXiv:1207.7214.

[3] B. Bellazzini, C. Csáki, and J. Serra, "Composite Higgses", *Eur. Phys. J. C* **74** (2014) 2766, doi:10.1140/epjc/s10052-014-2766-x, arXiv:1401.2457.

[4] R. Contino, D. Marzocca, D. Pappadopulo, and R. Rattazzi, "On the effect of resonances in composite Higgs phenomenology", *JHEP* **10** (2011) 081, doi:10.1007/JHEP10(2011)081, arXiv:1109.1570.

[5] D. Marzocca, M. Serone, and J. Shu, "General Composite Higgs Models", *JHEP* **08** (2012) 013, doi:10.1007/JHEP08(2012)013, arXiv:1205.0770.

[6] T. Han, H. E. Logan, B. McElrath, and L.-T. Wang, "Phenomenology of the little Higgs model", *Phys. Rev. D* **67** (2003) 095004, doi:10.1103/PhysRevD.67.095004, arXiv:0301040.

[7] M. Schmaltz and D. Tucker-Smith, "Little Higgs review", *Ann. Rev. Nucl. Part. Sci.* **55** (2005) 229–270, doi:10.1146/annurev.nucl.55.090704.151502, arXiv:hep-ph/0502182.

[8] M. Perelstein, "Little Higgs models and their phenomenology", *Prog. Part. Nucl. Phys.* **58** (2007) 247–291, doi:10.1016/j.ppnp.2006.04.001, arXiv:hep-ph/0512128.

[9] D. Pappadopulo, A. Thamm, R. Torre, and A. Wulzer, "Heavy vector triplets: bridging theory and data", *JHEP* **09** (2014) 60, doi:10.1007/JHEP09(2014)060, arXiv:1402.4431.

[10] CMS Collaboration, "Search for new resonances decaying via WZ to leptons in proton-proton collisions at $\sqrt{s} = 8$ TeV", *Phys. Lett. B* **740** (2015) 83, doi:10.1016/j.physletb.2014.11.026, arXiv:1407.3476.

[11] ATLAS Collaboration, "Search for WZ resonances in the fully leptonic channel using pp collisions at $\sqrt{s} = 8$ TeV with the ATLAS detector", *Phys. Lett. B* **737** (2014) 223, doi:10.1016/j.physletb.2014.08.039, arXiv:1406.4456.

[12] ATLAS Collaboration, "Search for resonant diboson production in the $\ell\ell q\bar{q}$ final state in pp collisions at $\sqrt{s} = 8$ TeV with the ATLAS detector", *Eur. Phys. J. C* **75** (2015), no. 2, 69, doi:10.1140/epjc/s10052-015-3261-8, arXiv:1409.6190.

[13] ATLAS Collaboration, "Search for resonant diboson production in the WW/WZ $\to \ell\nu$jj decay channels with the ATLAS detector at $\sqrt{s} = 7$ TeV", *Phys. Rev. D* **87** (2013) 112006, doi:10.1103/PhysRevD.87.112006, arXiv:1305.0125.

[14] CMS Collaboration Collaboration, "Search for massive resonances in dijet systems containing jets tagged as W or Z boson decays in pp collisions at $\sqrt{s} = 8$ TeV", *JHEP* **08** (2014) 173, doi:10.1007/JHEP08(2014)173, arXiv:1405.1994.

[15] G. Altarelli, B. Mele, and M. Ruiz-Altaba, "Searching for new heavy vector bosons in p colliders", *Z. Phys. C* **45** (1989) 109, doi:10.1007/BF01556677. Erratum-ibid. C 47.

[16] CMS Collaboration, "Search for massive resonances decaying into pairs of boosted bosons in semi-leptonic final states at $\sqrt{s} = 8$ TeV", *JHEP* **08** (2014) 174, doi:10.1007/JHEP08(2014)174, arXiv:1405.3447.

[17] CMS Collaboration, "Search for narrow high-mass resonances in proton-proton collisions at sqrt(s) = 8 TeV decaying to Z and Higgs bosons", (2015). arXiv:1502.04994. Submitted to Phys. Lett. B.

[18] M. Gouzevitch et al., "Scale-invariant resonance tagging in multijet events and new physics in Higgs pair production", *JHEP* **07** (2013) 148, doi:10.1007/JHEP07(2013)148, arXiv:1303.6636.

[19] CMS Collaboration, "Performance of b tagging at $\sqrt{s} = 8$ TeV in multijet, $\mathrm{t\bar{t}}$ and boosted topology events", CMS Physics Analysis Summary CMS-PAS-BTV-13-001, 2013.

[20] CMS Collaboration, "Study of Jet Substructure in pp Collisions at 7 TeV in CMS", CMS Physics Analysis Summary CMS-PAS-JME-10-013, 2010.

[21] CMS Collaboration, "Identification techniques for highly boosted W bosons that decay into hadrons", *JHEP* **12** (2014) 017, doi:10.1007/JHEP12(2014)017, arXiv:1410.4227.

[22] CMS Collaboration, "The CMS experiment at the CERN LHC", *JINST* **3** (2008) S08004, doi:10.1088/1748-0221/3/08/S08004.

[23] J. Alwall et al., "MadGraph 5: Going Beyond", *JHEP* **06** (2011) 128, doi:10.1007/JHEP06(2011)128, arXiv:1106.0522.

[24] D. Pappadopulo, A. Thamm, R. Torre, and A. Wulzer, "Resources for Heavy Vector Triplets",.

[25] GEANT4 Collaboration, "GEANT4 – a simulation toolkit", *Nucl. Instrum. Meth. A* **506** (2003) 250, doi:10.1016/S0168-9002(03)01368-8.

[26] T. Sjöstrand, S. Mrenna, and P. Skands, "PYTHIA 6.4 physics and manual", *JHEP* **05** (2006) 026, doi:10.1088/1126-6708/2006/05/026, arXiv:hep-ph/0603175.

[27] S. Gieseke et al., "Herwig++ 2.5 Release Note", arXiv:1102.1672.

[28] R. Field, "Early LHC Underlying Event Data – Findings and Surprises", in *Proceeedings of the Hadron Collider Physics Symposium*. 2010. arXiv:1010.3558.

[29] J. Pumplin et al., "New generation of parton distributions with uncertainties from global QCD analysis", *JHEP* **07** (2002) 012, doi:10.1088/1126-6708/2002/07/012, arXiv:hep-ph/0201195.

[30] CMS Collaboration, "Particle–Flow Event Reconstruction in CMS and Performance for Jets, Taus, and $E_{\mathrm{T}}^{\mathrm{miss}}$", CMS Physics Analysis Summary CMS-PAS-PFT-09-001, 2009.

[31] CMS Collaboration, "Commissioning of the Particle-flow Event Reconstruction with the first LHC collisions recorded in the CMS detector", CMS Physics Analysis Summary CMS-PAS-PFT-10-001, 2010.

[32] M. Wobisch and T. Wengler, "Hadronization corrections to jet cross-sections in deep inelastic scattering", (1998). arXiv:hep-ph/9907280.

[33] Y. L. Dokshitzer, G. D. Leder, S. Moretti, and B. R. Webber, "Better jet clustering algorithms", *JHEP* **08** (1997) 001, doi:10.1088/1126-6708/1997/08/001, arXiv:hep-ph/9707323.

[34] M. Cacciari and G. P. Salam, "Dispelling the N^3 myth for the k_t jet-finder", *Phys. Lett. B* **641** (2006) 57, doi:10.1016/j.physletb.2006.08.037, arXiv:hep-ph/0512210.

[35] M. Cacciari, G. P. Salam, and G. Soyez, "FastJet User Manual", *Eur. Phys. J. C* **72** (2012) 1896, doi:10.1140/epjc/s10052-012-1896-2, arXiv:1111.6097.

[36] M. Cacciari, G. P. Salam, and G. Soyez, "The Catchment Area of Jets", *JHEP* **04** (2008) 005, doi:10.1088/1126-6708/2008/04/005, arXiv:0802.1188.

[37] M. Cacciari and G. P. Salam, "Pileup subtraction using jet areas", *Phys. Lett. B* **659** (2008) 119, doi:10.1016/j.physletb.2007.09.077, arXiv:0707.1378.

[38] CMS Collaboration, "Determination of Jet Energy Calibration and Transverse Momentum Resolution in CMS", *JINST* **6** (2011) P11002, doi:10.1088/1748-0221/6/11/P11002, arXiv:1107.4277.

[39] CMS Collaboration, "Jet Performance in pp Collisions at $\sqrt{s}$=7 TeV", CMS Physics Analysis Summary CMS-PAS-JME-10-003, 2010.

[40] CMS Collaboration Collaboration, "Search for narrow resonances using the dijet mass spectrum in pp collisions at $\sqrt{s}$=8TeV", *Phys. Rev. D* **87** (2013) 114015, doi:10.1103/PhysRevD.87.114015, arXiv:1302.4794.

[41] S. D. Ellis, C. K. Vermilion, and J. R. Walsh, "Techniques for improved heavy particle searches with jet substructure", *Phys. Rev. D* **80** (2009) 051501, doi:10.1103/PhysRevD.80.051501, arXiv:0903.5081.

[42] S. D. Ellis, C. K. Vermilion, and J. R. Walsh, "Recombination Algorithms and Jet Substructure: Pruning as a Tool for Heavy Particle Searches", *Phys. Rev. D* **81** (2010) 094023, doi:10.1103/PhysRevD.81.094023, arXiv:0912.0033.

[43] CMS Collaboration, "Identification of b-quark jets with the CMS experiment", *JINST* **8** (2013) 04013, doi:10.1088/1748-0221/8/04/P04013, arXiv:1211.4462.

[44] M. Cacciari, G. P. Salam, and G. Soyez, "The anti-k_t jet clustering algorithm", *JHEP* **04** (2008) 063, doi:10.1088/1126-6708/2008/04/063, arXiv:0802.1189.

[45] J. Thaler and K. Van Tilburg, "Identifying Boosted Objects with N-subjettiness", *JHEP* **03** (2011) 015, doi:10.1007/JHEP03(2011)015, arXiv:1011.2268.

[46] J. Thaler and K. Van Tilburg, "Maximizing Boosted Top Identification by Minimizing N-subjettiness", *JHEP* **02** (2012) 093, doi:10.1007/JHEP02(2012)093, arXiv:1108.2701.

[47] I. W. Stewart, F. J. Tackmann, and W. J. Waalewijn, "N-Jettiness: An Inclusive Event Shape to Veto Jets", *Phys. Rev. Lett.* **105** (2010) 092002, doi:10.1103/PhysRevLett.105.092002, arXiv:1004.2489.

[48] CMS Collaboration, "Search for massive resonances in dijet systems containing jets tagged as W or Z boson decays in pp collisions at $\sqrt{s}$ = 8 TeV", *JHEP* **08** (2014) 173, doi:10.1007/JHEP08(2014)173, arXiv:1405.1994.

[49] R. G. Lomax and D. L. Hahs-Vaughn, "Statistical Concepts: A Second Course". p.10, Routledge Academic, third edition, 2007.

[50] G. Punzi, "Sensitivity of Searches for New Signals and Its Optimization", in *Statistical Problems in Particle Physics, Astrophysics, and Cosmology*, L. Lyons, R. Mount, and R. Reitmeyer, eds., p. 79. 2003. arXiv:physics/0308063.

[51] CMS Collaboration, "Status of the 8 TeV Jet Energy Corrections and Uncertainties based on 11/fb of data in CMS", *CMS Detector Performance Notes* **DP-2013/011** (2013).

[52] CMS Collaboration, "CMS Luminosity Based on Pixel Cluster Counting - Summer 2013 Update", CMS Physics Analysis Summary CMS-PAS-LUM-13-001, 2013.

[53] H.-L. Lai et al., "New parton distributions for collider physics", *Phys. Rev. D* **82** (2010) 074024, doi:10.1103/PhysRevD.82.074024, arXiv:1007.2241.

[54] A. Martin, W. Stirling, R. Thorne, and G. Watt, "Parton distributions for the LHC", *Eur. Phys. J. C* **63** (2009) 189, doi:10.1140/epjc/s10052-009-1072-5, arXiv:0901.0002.

[55] NNPDF Collaboration, "Fitting Parton Distribution Data with Multiplicative Normalization Uncertainties", *JHEP* **05** (2010) 075, doi:10.1007/JHEP05(2010)075, arXiv:0912.2276.

[56] S. Alekhin et al., "The PDF4LHC Working Group Interim Report", arXiv:1101.0536.

[57] G. Cowan, K. Cranmer, E. Gross, O. Vitells, "Asymptotic formulae for likelihood based tests of new physics", *Eur. Phys. J.* **C71** (2011) 1554, arXiv:physics/1007.1727.

[58] A. L. Read, "Presentation of search results: The CL_s technique", *J. Phys. G* **28** (2002) 2693, doi:10.1088/0954-3899/28/10/313.

[59] T. Junk, "Confidence level computation for combining searches with small statistics", *Nucl. Instrum. Meth. A* **434** (1999) 435, doi:10.1016/S0168-9002(99)00498-2, arXiv:hep-ex/9902006.